

# Catalysis Science & Technology

Accepted Manuscript



This is an *Accepted Manuscript*, which has been through the Royal Society of Chemistry peer review process and has been accepted for publication.

*Accepted Manuscripts* are published online shortly after acceptance, before technical editing, formatting and proof reading. Using this free service, authors can make their results available to the community, in citable form, before we publish the edited article. We will replace this *Accepted Manuscript* with the edited and formatted *Advance Article* as soon as it is available.

You can find more information about *Accepted Manuscripts* in the [Information for Authors](#).

Please note that technical editing may introduce minor changes to the text and/or graphics, which may alter content. The journal's standard [Terms & Conditions](#) and the [Ethical guidelines](#) still apply. In no event shall the Royal Society of Chemistry be held responsible for any errors or omissions in this *Accepted Manuscript* or any consequences arising from the use of any information it contains.

## ARTICLE

## Efficient Nitrogen-13 Radiochemistry catalyzed by a Highly Stable Immobilized Biocatalyst

Cite this: DOI: 10.1039/x0xx00000x

Eunice S. da Silva<sup>a</sup>, Vanessa Gómez-Vallejo<sup>b</sup>, Jordi Llop<sup>a,\*</sup> and Fernando López-Gallego<sup>c,d,\*</sup>

Received 00th January 2015,  
Accepted 00th January 2015

DOI: 10.1039/x0xx00000x

www.rsc.org/

The continuous progress of nuclear imaging techniques demands the development and implementation of efficient, clean and sustainable synthetic routes for the preparation of novel radiotracers. This is especially challenging in the context of radiotracers labelled with short-lived positron emitters such as Nitrogen-13. Biocatalysis can offer attractive alternatives to conventional chemistry, because enzymes present an exquisite chemical selectivity and high turnover numbers. However enzymes have been poorly exploited in the area of radiochemistry. Herein, we present the design and fabrication of an heterogeneous biocatalyst suitable for the reduction of [<sup>13</sup>N]NO<sub>3</sub><sup>-</sup> into [<sup>13</sup>N]NO<sub>2</sub><sup>-</sup>. A eukaryotic nitrate reductase from *Aspergillus niger* has been immobilized on different carriers and immobilization parameters were determined. Optimal results were obtained for agarose beads activated with positively charged tertiary amino group (Ag-DEAE). The immobilized preparation was 12-fold more thermostable than the soluble enzyme. Biochemical characterization of the immobilized enzyme showed an interesting thermal-induced hyperactivation driven by the interaction between the enzyme and the carrier. The heterogeneous biocatalyst could be re-used up to 7 reaction cycles preserving its initial activity. Finally, to demonstrate the potential of this heterogeneous biocatalyst in the context of radiochemistry, the radiosynthesis of *S*-[<sup>13</sup>N]nitrosoglutathione was approached using enzymatically produced [<sup>13</sup>N]NO<sub>2</sub><sup>-</sup> as the labelling agent.

**Keywords:** Positron emission tomography, Nitrogen-13, radiotracer, oxidoreductases, biocatalysis, immobilization

### Introduction

Recent advances in Positron Emission Tomography (PET) have encouraged chemists to synthesize novel radiotracers to enable the non-invasive diagnosis of a larger variety of diseases and the investigation of their molecular basis<sup>1</sup>. Due to the short half-life ( $T_{1/2}$ ) of the most commonly used positron emitters, i.e. Fluorine-18 (<sup>18</sup>F,  $T_{1/2}$  = 109.8 min), Carbon-11 (<sup>11</sup>C,  $T_{1/2}$  = 20.4 min) and Nitrogen-13 (<sup>13</sup>N,  $T_{1/2}$  = 9.97 min), the radiosynthesis of PET tracers requires the development of efficient chemical schemes in order to synthesize and purify the radioactive species in a short period of time<sup>2</sup>. Indeed, radiolabelling methods must be fast and highly efficient to perform chemical reactions and downstream processing in an appropriate time scale, preventing thus excessive radioactivity loss while improving the specific activity of the resulting radiotracers.

Biocatalysis can offer attractive solutions in the area of radiochemistry because enzymes present an exquisite chemical selectivity and high turnover numbers. Enzymes enable fast chemical conversions, and yield highly pure products under extremely mild conditions. However, whereas enzymes have been naturally evolved as soluble and labile catalysts, stability and solubility issues often limit their industrial applications. These issues may be circumvented by enzyme immobilization, that turns enzymes

into stable and heterogeneous biocatalysts<sup>3</sup>. In this context, appropriate selection of the solid carrier and immobilization chemistry is crucial to achieve highly active and stable heterogeneous enzymes that can be readily integrated to continuous processes.

There are a handful of examples where immobilized enzymes have been utilized for the synthesis of different <sup>18</sup>F- and <sup>11</sup>C-labelled radiotracers<sup>3-7</sup>. Nevertheless, the enzyme-assisted preparation of radiotracers labelled with shorter-lived positron emitters such as <sup>13</sup>N is more challenging and remains rather unexplored<sup>8</sup>. In fact, there are only a few examples where immobilized enzymes have been applied to the catalytic incorporation of <sup>13</sup>N into *L*-amino acids<sup>9-11</sup>.

Usually, <sup>13</sup>N is generated via the <sup>16</sup>O(p,α)<sup>13</sup>N nuclear reaction by proton irradiation of pure water. Nitrogen-13 is formed as a mixture of <sup>13</sup>N-labelled nitrate ([<sup>13</sup>N]NO<sub>3</sub><sup>-</sup>), nitrite ([<sup>13</sup>N]NO<sub>2</sub><sup>-</sup>) and ammonia ([<sup>13</sup>N]NH<sub>3</sub>), being [<sup>13</sup>N]NO<sub>3</sub><sup>-</sup> the major species (~85% of total radioactivity); if a radical scavenger (e.g. 5mM ethanol) is added to the irradiated water, [<sup>13</sup>N]NH<sub>3</sub> is the major species. As recently shown by our research group, the labelling agent [<sup>13</sup>N]NO<sub>2</sub><sup>-</sup> is a useful precursor for the preparation of a wide range of labelled compounds such as *S*-[<sup>13</sup>N]nitrosothiols<sup>12, 13</sup>, *S*-[<sup>13</sup>N]nitrosamines<sup>14</sup>, <sup>13</sup>N-labelled azo derivatives<sup>15, 16</sup> and <sup>13</sup>N-labelled azides<sup>17</sup>, and further applications are currently being investigated. Unfortunately, direct production of [<sup>13</sup>N]NO<sub>2</sub><sup>-</sup> in the cyclotron is not feasible and it is usually obtained by reduction of [<sup>13</sup>N]NO<sub>3</sub><sup>-</sup> to [<sup>13</sup>N]NO<sub>2</sub><sup>-</sup> on a column containing activated cadmium. Besides the inherent toxicity of cadmium, which may hamper the translation of the technology to the clinical arena, this experimental setting presents several technological pitfalls.

Inspired by the biological cycle of nitrogen, we reasoned that eukaryotic nitrate reductase (eNR) may efficiently catalyze the reduction of [<sup>13</sup>N]NO<sub>3</sub><sup>-</sup> to the more convenient labelling agent [<sup>13</sup>N]NO<sub>2</sub><sup>-</sup>. eNR is a homodimer which contains three different domains per monomer: one N-terminus domain that binds NADPH and FAD<sup>+</sup> as redox cofactors (NADPH-domain), a second cytochrome b domain containing a Fe-heme cofactor (heme-domain) and a third C-terminus domain that binds a molybdopterin cofactor (MOCO-domain). All these cofactors are required during the catalytic cycle; while FAD<sup>+</sup>, heme and MOCO cofactors are stably bound to the enzymes, NADPH must be exogenously added to the reaction media. The enzyme mechanism relies on the large conformational change that approaches the NADPH/FAD<sup>+</sup> and heme domains to the MOCO domain, allowing the electron transfer from NADPH to molybdenum via the heme group to reduce NO<sub>3</sub><sup>-</sup> to NO<sub>2</sub><sup>-18</sup>. Immobilization of this enzyme is rather challenging since restrictions in the conformational flexibility required for the catalysis may compromise the reducing capacity. This structural complexity may explain the low recovered activity of immobilized eNRs reported elsewhere<sup>19</sup>.

In the current work, we present the unprecedented use of eNR as an efficient heterogeneous biocatalysts for the reduction of [<sup>13</sup>N]NO<sub>3</sub><sup>-</sup> to [<sup>13</sup>N]NO<sub>2</sub><sup>-</sup>. The immobilization chemistry has been optimized to yield active and stable preparations of immobilized eNR on porous agarose beads. As a proof of concept of the applicability of the experimental set up to the preparation of PET tracers, the <sup>13</sup>N-labelled nitrosothiol *S*-[<sup>13</sup>N]nitrosoglutathione ([<sup>13</sup>N]GSNO) has been prepared with excellent radiochemical conversion.

## Results and discussion

### Immobilization of eNR on functionalized porous agarose beads

Eukaryotic Nitrate reductase (eNR) from *Aspergillus niger* was immobilized through different immobilization chemistries on a survey of agarose-based matrixes (see **Table 1**) with the same physical parameters (surface area, pore size and particle diameter) but having different functional groups on their surfaces. We screened several immobilization chemistries (reversible and irreversible) in order to find the optimal one in terms of both activity and stability of the resulting heterogeneous biocatalyst.

**Table 1. Parameters of *Aspergillus niger* nitrate reductase immobilization onto agarose carrier via different chemistries.**

CARRIER	Reactive group	Immobilization chemistry	Immobilized Activity $A_i$ (mU/g) <sup>a</sup>	Immobilization yield $\psi$ (%) <sup>b</sup>	Expressed Activity $A_e$ (mU/g) / (%) <sup>d</sup>
Ag-CB	Cyanogen Bromide	Covalent bond through the eNR Nt	964±32	96±3	26±4 / (3)
Ag-DEAE	Diethyl-aminoethyl		995±10	99±1	210±60 / (21)
Ag-PEI	Poly-ethylenimine	Ionic adsorption through the most acid eNR regions	982±12	98±1	155±25 / (16)
Ag-MANAE	Mono-aminoethyl		820±24	82±2	192±41 / (23)
Ag-DS	Dextran-sulphate	Ionic adsorption through the most basic eNR regions	750	75	58 / (8)

The initial offered activity was always 1000mU per gram. <sup>a</sup> $A_i$ =The activity immobilized on 1 gram of carrier after the immobilization process. This activity was calculated as the difference between the offered activity and the activity in the supernatant after incubation with the carrier for 1h. <sup>b</sup>Immobilization yield ( $\psi$ ) = (immobilized activity/offered activity) x 100. <sup>c</sup>The expressed activity ( $A_e$ ) is defined as the measured activity of the immobilized enzyme after washing. <sup>d</sup>Relative expressed activity ( $A_e$ ) = (expressed activity/immobilized activity) x 100.

Table 1 shows that all carriers were able to efficiently immobilize eNR (immobilization yields >75% in all cases), although low values of expressed activity were achieved after immobilization when compared to the free enzyme. Irreversible immobilization and cationic exchange on Ag-CB and Ag-DS led to a dramatic decrease in the expressed activity (26±4 and 58 mU/g, respectively). On the other hand, ionic immobilization of eNR on positively charged carriers yielded values of expressed activity in the range 155-210 mU/g, resulting in up to 23% of relative expressed activity. Noteworthy, although the chemistry that drove the immobilization on Ag-MANAE, Ag-DEAE and Ag-PEI was the same, Ag-MANAE offered lower immobilization yields (82±2%) than Ag-DEAE (99±1%) and Ag-PEI (98±1%). This fact may be explained because Ag-MANAE surface presents a lower density of positively charged groups than Ag-DEAE and Ag-PEI surfaces.

In order to explain the functional discrepancies obtained with the different immobilized preparations, we further studied the eNR surface to understand how the protein orientation on the carrier surface may affect its functionality. Unfortunately, X-ray structure of eNR from *A. niger* has not been solved yet, and hence its 3D-structural homology model containing the NADPH-domain, the heme-domain and the MOCO-domain was built (**Figure 1A**) and the electrostatic surface potential was calculated in order to determine the spatial charge distribution across the enzyme surface (**Figure 1B and 1C**). The analysis of this structural model reveals an acidic belt on the MOCO-domain located at the opposite face regarding to the active site. The model also shows that heme, FAD<sup>+</sup>, NAD<sup>+</sup> and molybdenum binding sites are surrounded by basic amino acids (**Figure 1C**). These structural observations suggest that eNR immobilized on Ag-DS is oriented through its active site (basic region), hampering the accessibility of both NADPH and nitrate to the catalytic pocket with consequent decrease in catalytic efficiency. Nevertheless, the eNR orientation onto positively charged carriers seems to occur through one acidic region located far away from the binding pockets. As a consequence, active centres remain fairly accessible for the substrates, resulting in significantly

higher relative expressed activity values for such immobilized preparations (**Figure 1C**). Moreover, such orientation seems to negligibly affect dimer stability because the dimerization domain is not involved in the protein-carrier interaction. In fact, when eNR immobilized on Ag-DEAE was incubated under high ionic strength conditions, enzymatic activity was quantitatively eluted to the supernatant, demonstrating the ionic character and the reversibility of this immobilization chemistry.

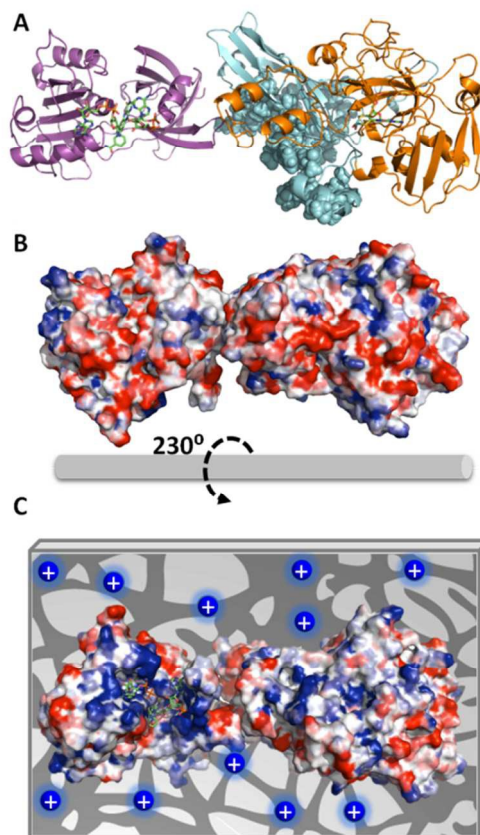


**Figure 1-Structural model of a monomer of eNR from *Aspergillus niger*.** (A) Cartoon representation of 3D-structural homology model by using the X-ray structures of eNR from *Pichia pastoris* and cytochrome B5 from rat complexed with both FAD<sup>+</sup> and NAD<sup>+</sup> as templates for molybdenum domain (N-terminus) (orange) and cytochrome domain (C-terminus) (purple) respectively. The sphere representation colored in cyan depicts the dimerization domain of the eNR. Green sticks represent the cofactors NAD<sup>+</sup>, FAD<sup>+</sup> and molybdopterin. (B) Surface electrostatic potential of eNR calculated by Blues server (back face of active site) and (C) proposed orientation of eNR monomer on porous Ag-DEAE surface. The blue circles represent the tertiary amine groups located on the carrier surface. The surface electrostatic potential is depicted with a red-blue gradient that correspond to the acid-basic gradient. All the images were prepared by using Pymol 0.99v.

The values of expressed activity shown in Table 1 have been determined by using NADPH as cofactor; such values are relatively high when compared to previous results obtained using immobilization protocols based on porous hydrogels. For example, eNR from *Aspergillus niger* immobilized on a porous vinyl polymeric matrix expressed less than 2% of its expressed activity by using NADPH as cofactor<sup>19</sup>. The high structural complexity of eNR might be the main reason for the low expressed activity achieved in this previous work. This enzyme requires enough structural flexibility for efficient electron transfer between both the cytochrome and the molybdenum domains. Hence, immobilization chemistries that highly rigidify the 3D structure of eNR (covalent immobilization), may hinder the catalytic conformational changes or promote wrong protein orientations that limit either the electron transfer or the substrate accessibility, resulting in a low expressed activity of the immobilized preparation.

**Effects of the temperature on both activity and stability of eNR immobilized on positively charged agarose beads**

The thermal stabilities of immobilized and soluble eNR were tested at different temperatures. **Figure 2A** shows the inactivation courses of the three different immobilized preparations incubated at pH=7.5 and 25°C. The half-life time of eNR immobilized on Ag-DEAE was estimated 30-fold and 6-fold higher than eNR immobilized on Ag-MANAE and Ag-PEI, respectively, suggesting a dependence of the thermal stability of the immobilized enzymes with the chemical nature of the amine groups located at the surface of the carrier. The surface of Ag-DEAE containing tertiary amine groups seems to establish more favourable interactions with the acidic protein regions than the Ag-MANAE surface, which presents low density of primary amine groups, and the Ag-PEI surface coated by a polymeric bed with a high density of primary, secondary and tertiary amine groups. Ag-PEI has been suggested as an excellent carrier to stabilize multimeric enzymes, because the basic polymeric bed establishes 3D-protein-polymer interactions<sup>20</sup> that attach all the subunits to the carrier, resulting in a stabilization of the quaternary structure of the protein. Unexpectedly, in this study, eNR immobilized on Ag-PEI was less stable than eNR immobilized on Ag-DEAE. This unexpected result may be explained because the flexibility of the polymer may generate additional interactions with the protein over time. Such enhancement of the spatial reactivity may lead to undesired interactions between both cytochrome and molybdenum domains and the polymeric brushes, reducing the enzyme flexibility required for the electron transfer, and consequently decreasing the nitrate reduction activity over time. Those negative interactions would not be possible in the much less flexible Ag-DEAE surface formed by a 2D-monolayer of tertiary amine groups. Hence, our results suggest that the interaction between eNR and the positively charged carriers must be strong enough to guarantee the stabilizing immobilization effect and flexible enough to enable the conformation changes required for the catalysis.

The Ag-DEAE immobilized enzyme was much more stable than its soluble counterpart under a broad range of temperatures (30–55°C) (**Figure 2B**). Surprisingly, when such immobilized biocatalyst was incubated for only 15 minutes in the range of 40–45°C and the enzyme activity was assayed at 25°C, a 2-fold activity enhancement (hyperactivation) was observed with respect to the non-thermally treated enzyme (**Figure 2B**). This effect was not observed with the soluble enzyme, which decreased its initial activity after incubation at T>25°C due to thermal inactivation. Interestingly, both the soluble and immobilized enzymes showed similar activity/temperature profiles (**Figure S1**). Altogether, these results suggest that the aforementioned hyperactivation effect can only be attributed to the presence of the carrier and that is not related to the effect of the temperature on the catalysis itself. Inactivation kinetics studies (pH 7.5 and 40°C) of the hyperactivated immobilized enzyme proved an enhanced stability with respect to its soluble counterpart under the same conditions (**Figure S2**). The immobilized enzyme showed a thermal inactivation constant ( $K_i$ ) of  $(1.31 \pm 0.63) \times 10^{-5} \text{ (s}^{-1}\text{)}$  at 40°C, while the  $K_i$  value of the soluble enzyme was  $(15.3 \pm 2.3) \times 10^{-5} \text{ (s}^{-1}\text{)}$ . These values confirm that the immobilization process results in an increased half-life time ( $t_{1/2}$ ) of eNR up to 883 minutes; 12 times longer than the  $t_{1/2}$  of the soluble enzyme.

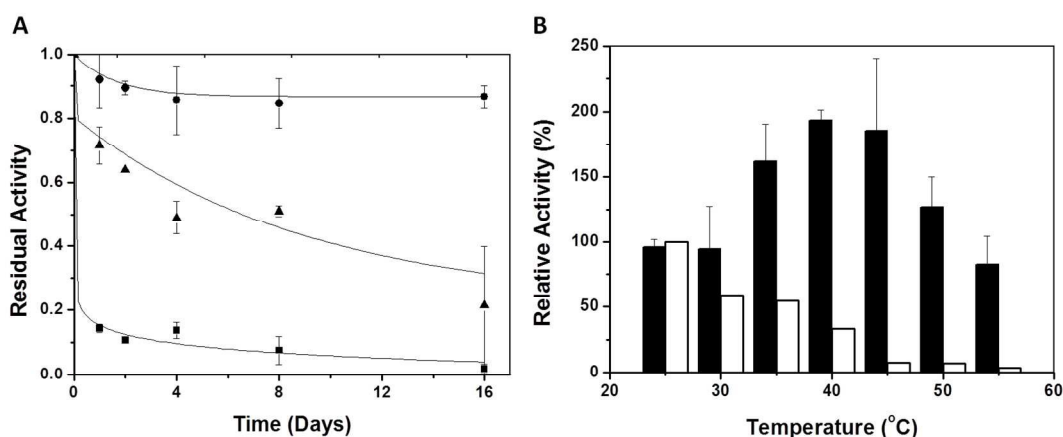


**Figure 2- Stability of eNR.** (A) Inactivation course of different eNR immobilized preparations at 25°C and pH 7.5. eNR was immobilized on Ag-DEAE (●); Ag-PEI (▲); Ag-MANAe (■). Values are normalized to starting activity. (B) Inactivation of eNR soluble (white bars) and immobilized on Ag-DEAE (black bars) at different temperatures. Soluble and immobilized preparations were incubated 15 minutes at different temperatures and then activities were assayed at 25 °C.

The thermal-hyperactivation and thermal-stabilization effects observed for eNR immobilized on Ag-DEAE may be explained by some beneficial enzyme-carrier interactions that drive to some local structural re-organization in the enzyme, resulting in a more efficient electron transfer between the NADPH and the MOCO domains. Those interactions may stabilize a more beneficial conformation for eNR, which explains the 2-fold more active and 12-fold more stable enzyme. These carrier- and temperature-assisted conformational changes were further investigated by fluorescence studies that suggested a relationship between the improved functional properties and a structural reorganization (**Supporting information, figure S3**). Indeed, alterations in the fluorescence spectrum of the immobilized enzyme were observed with increased temperature, while no changes were observed for the soluble enzyme incubated under the same conditions. Hereby, the temperature seems to act as an external stimulus that induces an optimal fitting between the surfaces of the enzyme and the carrier, resulting in a suitable geometric congruence for the catalysis. Despite the nature of this thermally-induced more active conformation is not clear at present, it is worth mentioning that similar effects have been described for other thermostable soluble enzymes<sup>21-23</sup>. In any case, we put forth one of the few experimental demonstrations of thermal hyperactivation and stabilization assisted by the carrier surface, which is not only acting as a scaffold to stabilize eNR but also as an active surface that induces temperature-triggered positive conformational changes on the enzyme.

### Kinetic parameters and loading capacity of eNR immobilized on Ag-DEAE

Based on both the high stability and acceptable catalytic efficiency of eNR immobilized on Ag-DEAE, we selected this heterogeneous biocatalyst to carry out the sustainable reduction of  $[^{13}\text{N}]\text{NO}_3^-$  to  $[^{13}\text{N}]\text{NO}_2^-$  in aqueous media under mild conditions. However, before applying this biocatalyst to radiochemistry, we carried out its kinetic characterization. To this aim, Michaelis-Menten parameters were determined for both soluble and the immobilized eNRs towards both nitrate and NADPH (**Table 2**).

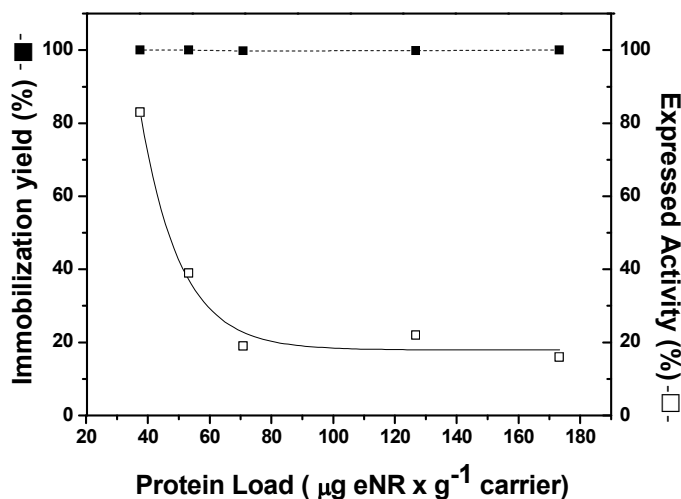
Kinetic studies provided us interesting data that helped to understand the activity decrease resulting from the immobilization process. In a first glance, the immobilized preparation showed a 26-fold  $K_{\text{m}[\text{NADPH}]}$  higher than the soluble enzyme. Contrarily,  $K_{\text{m}[\text{NO}_3]}$  was 4.5 times smaller for the immobilized eNR than for the soluble preparation. These results confirm that immobilization of eNR on Ag-DEAE negatively affected the enzyme binding towards NADPH, which explains the low expressed activity after the immobilization process. The high  $K_{\text{m}[\text{NADPH}]}$  values for the immobilized preparation may due to two main reasons: i) Conformational changes induced by the carrier during the immobilization process that diminish the enzyme affinity towards NADPH, or ii) mass transfer issues that hamper NADPH diffusivity from the bulk solution to the active sites of the immobilized eNR molecules.

Table 2. Kinetic characterization of free and immobilized *Aspergillus niger* eNRs.

		K <sub>m</sub> (mM)	k <sub>cat</sub> (s <sup>-1</sup> )	K <sub>cat</sub> /K <sub>m</sub> (s <sup>-1</sup> • mM <sup>-1</sup> )
NaNO <sub>3</sub>	NR soluble	0.27±0.07	30.33	111.23
	NR Ag-DEAE	0.06±0.03	11.97	199.44
NADPH	NR free	0.07±0.03	27.93	399.05
	NR Ag-DEAE	1.86±0.82	N.D.	N.D.

The steady-state kinetics parameters were measured at pH 7.5 and 25°C (see Section *Material and Methods*).

In order to elucidate which reason contributes more to the low expressed activity, the effect of the enzyme loading on both immobilization yield and expressed activity after the immobilization was tested. Figure 3 shows that the immobilization was always quantitative regardless the enzyme load. However, the relative expressed activity presented a strong negative logarithmic correlation with the enzyme load. Under very low enzyme loads (37.5 μg<sub>eNR</sub>/g<sub>carrier</sub>) the relative expressed activity was 85%, while the value decreased to approximately 20% at loads higher than 75 μg<sub>eNR</sub>/g<sub>carrier</sub> (Figure 3).



**Figure 3 - Enzyme-loading capacity of Ag-DEAE.** The experiment was carried out offering different protein concentrations to 200mg of carrier at pH 7.5 and 25°C. Immobilization yield (full square) and relative expressed activity (open square) were determined for each enzyme load. Immobilization yield and expressed activity were calculated as was previously described in Table 1.

This experiment demonstrates that immobilization chemistry does not promote inactive enzyme conformations that intrinsically diminish its specific activity after the immobilization process. In such scenario, the expressed activity should be always low regardless of the enzyme load. Therefore, it is plausible to think that mass transfer limitations of substrate and cofactors are the main reason to explain the low expressed activity of the immobilized eNR. Contextualizing these results together with the high  $K_{m[NADPH]}$  values for the immobilized preparation, we suggest that the cofactor undergoes severe mass transfer limitations to diffuse across the Ag-DEAE microstructure to reach the enzyme active sites. Under high enzyme loads, NADPH does not efficiently diffuse into the porous microstructure of the carrier to saturate all active sites immobilized on such carrier. On the contrary, under very low enzyme loads, the vast majority of the eNR molecules are saturated with the NADPH. These results are in good agreement with previous data<sup>24</sup>, which showed that eNR from *A. niger* covalently immobilized on non-porous particles expresses more than 90% of its specific activity after immobilization. Moreover, they strongly suggest that low specific activity of eNR immobilized on positively charged agarose beads is due to limited NADPH diffusion rather than inaccurate protein orientation, because positively charged porous carrier seem to immobilize eNR through an optimal orientation according to the protein surface analysis (Figure 1C).



**Reduction of radiolabelled nitrate catalyzed by eNR immobilized on Ag-DEAE. Reusability of the immobilized biocatalyst**

eNR immobilized on Ag-DEAE was used to reduce  $[^{13}\text{N}]\text{NO}_3^-$  to  $[^{13}\text{N}]\text{NO}_2^-$ . The reaction was carried out in batch mode and the immobilized biocatalyst was re-used for several reaction cycles (**Figure 4**). In the first cycle the immobilized enzyme only yielded 60% of  $[^{13}\text{N}]\text{NO}_2^-$  in 4 minutes while the soluble enzyme reduced 96% of  $[^{13}\text{N}]\text{NO}_3^-$  to  $[^{13}\text{N}]\text{NO}_2^-$ . Surprisingly, in the second cycle the immobilized enzyme reduced up to 93% of  $[^{13}\text{N}]\text{NO}_3^-$  to  $[^{13}\text{N}]\text{NO}_2^-$ . We suggest that differences in NADPH effective concentration inside the carrier pores might cause that intriguing effect.

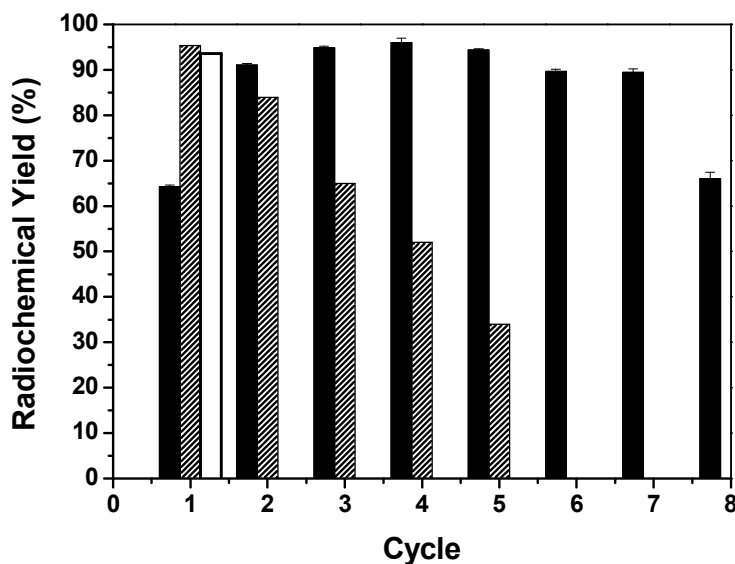


**Figure 4 - Reusability of eNR immobilized on Ag-DEAE.** Soluble eNR (white bar), eNR immobilized on Ag-DEAE without NADPH equilibration (black bars) and eNR immobilized on Ag-DEAE equilibrated with NADPH (stripped bars) were used to catalyze the reduction from  $[^{13}\text{N}]\text{NO}_3^-$  to  $[^{13}\text{N}]\text{NO}_2^-$  at 25° C and pH 7.5. Reactions catalyzed by soluble and non-equilibrated immobilized eNR were carried out by adding exogenous NADPH, while the reactions catalyzed by equilibrated immobilized eNR were carried out without adding exogenous NADPH.

We hypothesize that during the first reaction cycle some negatively charged NADPH molecules are ionically absorbed to the positively charged carrier surface. However, such molecules would present an association/dissociation equilibrium that would simultaneously provide one fraction of soluble NADPH available for the enzyme catalysis and a second fraction of NADPH trapped on the carrier surface that would be re-used in consecutive cycles. In this scenario, the effective concentration of NADPH in the second and successive cycles will be higher, explaining the higher yield observed in the second cycle compared to the first one. In order to demonstrate this ionic interaction between NADPH and Ag-DEAE, we equilibrated the eNR immobilized on Ag-DEAE with NADPH in solution before triggering the first reaction cycle. The equilibrated heterogeneous biocatalyst was able to reduce 96% of  $[^{13}\text{N}]\text{NO}_3^-$  to  $[^{13}\text{N}]\text{NO}_2^-$  from the first cycle (**Figure 4**). Moreover, we directly demonstrated that NADPH was bound to the carrier by analyzing the NADPH fluorescence inside the solid particles of the heterogeneous biocatalyst (**Figure S4**). These experimental evidences confirm that a fraction of NADPH is ionically trapped into the carrier surface, increasing the internal concentration of NADPH that results in higher reduction yields. In fact, when the radiochemical reduction was carried out with the NADPH-equilibrated immobilized enzyme, the heterogeneous biocatalyst was able to catalyze the radiolabelled nitrate reduction for 5 cycles with more than 30% yield without exogenous addition of NADPH (**Figure 4**). This experiment provides evidence that NADPH molecules are reversibly bound to the carrier surface providing an internal cofactor concentration that was sufficient for the immobilized eNR to catalyze the radiochemical reduction with the maximum yield during the first cycle, and proportionally lower yields with the consecutive cycles. The lower reduction yield along the cycles agrees with the fact that

NADPH is oxidized to NADP<sup>+</sup> decreasing the pool of NADPH trapped into the carrier porous structure. Therefore, along the consecutive cycles, immobilized eNR suffers from a lower availability of the reduced NADPH, explaining the lower yields along the operational cycles. Contrarily, when reduction was carried out by adding exogenous NADPH in each reaction cycle, the maximum yield was maintained during 7 cycles, demonstrating the excellent operational stability of the immobilized biocatalyst (**Figure 4**). As far as we know, this is the first evidence of a heterogeneous biocatalyst where the carrier plays an important role on supplying the corresponding cofactor to the enzyme. Furthermore, this optimal heterogeneous biocatalyst, offers a clean final product without any significant protein contamination, even during the recycling process (**Figure S5**), confirming once again that ionic interactions between eNR and Ag-DEAE are quite strong in spite of their reversible nature.

### Two step chemo-enzymatic solid-phase synthesis of *S*-[<sup>13</sup>N]GSNO

To proof the concept that the enzymatically synthesized [<sup>13</sup>N]NO<sub>2</sub><sup>-</sup> can be directly integrated into a radiochemical synthetic cascade, we coupled the optimal eNR immobilized on Ag-DEAE to the two-step chemo-enzymatic synthesis of *S*-[<sup>13</sup>N]GSNO (**Figure S6**). [<sup>13</sup>N]NO<sub>3</sub><sup>-</sup> was enzymatically reduced to [<sup>13</sup>N]NO<sub>2</sub><sup>-</sup> in the presence of NADPH. The supernatant of such reaction was passed through an anion exchange cartridge in order to trap the enzymatically produced [<sup>13</sup>N]NO<sub>2</sub><sup>-</sup>. Then, an acidic solution of *S*-glutathione (1 mM) was also passed through the same anion exchange cartridge enabling the solid-phase *S*-nitrosation of glutathione. The resulting product was finally desorbed from the resin by elution with distilled water. 95% of the enzymatically yielded [<sup>13</sup>N]NO<sub>2</sub><sup>-</sup> was converted to *S*-[<sup>13</sup>N]GSNO, similar to the radiochemical conversion obtained in our previous work using Cd-reduced [<sup>13</sup>N]NO<sub>2</sub><sup>-</sup>. This result confirms that the redox cofactor needed for the enzymatic reactions does not interfere with the next chemical step. Therefore, the radioactive nitrite produced by this heterogeneous biocatalyst is suitable to be used in radiochemical reactions.

## Experimental

### Materials.

Agarose beads activated with a primary amine group (Ag-MANAE)<sup>25, 26</sup>, coated with 25 KDa polyetheleneimine (Ag-PEI)<sup>20</sup> and coated with dextran-sulphate (Ag-DS)<sup>27</sup> were prepared as described elsewhere. Cyanogen bromide-activated-Sepharose® 4B (Ag-CB) was purchased from Sigma-Aldrich Química S.A. (Madrid, Spain) and DEAE-Sepharose was purchased from GE healthcare (Pittsburgh, USA). Nitrate reductase from *Aspergillus niger* and reduced β-Nicotinamide adenine dinucleotide 2'-phosphate tetrasodium salt (β-NADPH; purity >97%) were purchased from Roche Life Science (Barcelona, Spain). Sodium nitrite (NaNO<sub>2</sub>, ACS reagent, Ph. Eur.), sodium nitrate (NaNO<sub>3</sub>, ACS reagent), sodium phosphate dibasic (Na<sub>2</sub>HPO<sub>4</sub>, for molecular biology, purity ≥98.5%), sodium phosphate monobasic (NaH<sub>2</sub>PO<sub>4</sub>, purity ≥99.0%), glutathione (GSH, purity ≥99%), *S*-nitrosoglutathione (GSNO, purity ≥97%), hydrochloric acid (HCl, 1 M standard solution), sodium hydroxide (NaOH, ACS reagent), trifluoroacetic acid (CF<sub>3</sub>COOH, HPLC grade) and acetonitrile (CH<sub>3</sub>CN, HPLC grade) were purchased from Sigma-Aldrich Química S.A. (Madrid, Spain) and used without further purification. Bio-Rad Protein Assay Dye Reagent Concentrate was purchased from BIO-RAD (Madrid, Spain). Additive for ionic chromatography mobile phase (P/N 5062-2480) was purchased from Agilent Technologies (Madrid, Spain). All others reagents were of analytical grade unless otherwise specified.

### Methods.

**Structural modelling of nitrate reductase from *Aspergillus niger*.** Structural homology models complexed with molybdenum, NADPH, FAD<sup>+</sup> and heme cofactors were built by using different structural templates and aided by the homology-modeling server from ExPASy<sup>28</sup>. The modeling server selected the nitrate reductase from *Pichia pastoris* (2BIH) complexed with molybdopterin as template to model the molybdenum binding domain (56% identity). However, the server modeled both cytochrome and NADPH/FAD<sup>+</sup> domains by using NADH-dependent cytochrome B5 reductase from rat (1IB0) complexed with both FAD<sup>+</sup> and NAD<sup>+</sup> as template (39% identity). Structures are

validated by comparison of an atomic model with their amino acid sequences and assignment of positive (good compatibility) or negative scores for each amino acid positions. The model for the domain that binds NADPH, FAD<sup>+</sup> and heme has a very good compatibility score, while the model for the molybdenum binding domain presented very low score mainly due to the low compatibility of its N-terminus that was highly flexible and consequently hard to model. Protein models were visualized and aligned with their template structure by using PyMol 0.99 developed by DeLano Scientific LLC (San Francisco, CA). The electrostatic potential was calculated by using Blues server<sup>29</sup>.

**Determination of the enzyme activity and protein concentration.** The activities of both free and immobilized nitrate reductase (eNR) from *Aspergillus niger* were determined by measuring the decrease in absorbance at 340 nm, resulting from NADPH oxidation during the enzymatic conversion of nitrate to nitrite. A sample of enzyme solution (10 µL) was incubated in a multi-well plate with 190 µL reaction mixture (final concentration: 10 mM sodium phosphate buffer, 0.21 mM NADPH and 4.25 mM NaNO<sub>3</sub>, pH = 7.5) at 25°C under mild shaking. When indicated, different temperatures and pH values were used. One activity unit was defined as the amount of enzyme required to oxidize 1 µmol of NADPH under the above described conditions. The kinetic parameters were calculated from the initial rate values determined with different concentrations of NADPH (0-2 mM) and nitrate (0-20 mM). Results were fitted to Michaelis-Menten equation by non-linear regression and  $K_M$  and  $k_{cat}$  were calculated. Finally, the protein concentration of all soluble eNR samples was measured by using Bradford's method<sup>30</sup> and bovine serum albumin (BSA) as protein standard.

**Enzyme Immobilization.** The immobilization was carried out by adding 200mg of the corresponding carrier to 1mL of soluble eNR (1-5U/mL) in 10 mM sodium phosphate at pH= 7.5. The suspension was kept under mild stirring at 25°C. Periodically, samples of the supernatants and the carrier-enzyme suspensions were withdrawn and analyzed to evaluate the progress of the immobilization process. In parallel, a blank of the soluble enzyme (without carrier) was also analyzed. After immobilization, enzyme preparations were washed with an excess of distilled water and immobilization buffer to eliminate any non-bound protein molecule.

**Loading capacity of the Ag-DEAE.** Different amounts of *Aspergillus niger* eNR preparation (0.0075; 0.0107; 0.0143; 0.0255; 0.0349 mg protein) were offered to 200 mg of Ag-DEAE suspended in 1 mL of 10 mM sodium phosphate buffer at pH 7.5. The amount of protein bound to the carrier was determined as the difference between the initial and the residual protein concentration in the supernatants. This loading capacity was also monitored by analyzing both initial and residual enzyme activity in the supernatant.

**Characterization of free and immobilized *Aspergillus niger* eNR.** Different enzyme preparations (both soluble and immobilized), were incubated in 10mM sodium phosphate buffer (pH=7.5) at different temperatures (25-55°C) for 15 min. The eNR activities were assayed at 25 °C as previously described. In a different experiment, soluble and immobilized preparations were incubated at 40 °C, and samples were withdrawn at different times and assayed at 25°C to determine the residual activity. Reusability of eNR immobilized on Ag-DEAE was evaluated by performing consecutive catalytic cycles at 25°C using nitrate (both non-radioactive and radioactive) and NADPH as substrates. After each cycle, the immobilized preparation was washed and the enzymatic activity towards non-radioactive nitrate was determined by spectrophotometry, while the final yield towards radioactive nitrate was determined by radio-HPLC (see section *Radiochemistry*).

**Fluorescence Spectroscopy.** Fluorescence measurements were carried out in a Varioskan Flash fluorescence spectrophotometer (Thermo Scientific), monitoring the intrinsic tryptophan fluorescence of immobilized *A. niger* eNR, using an excitation wavelength of 280 nm with excitation and emission bandwidths of 5 nm and recording fluorescence emission spectrum between 300 and 600 nm. All spectroscopic measurements were made in 10 mM sodium phosphate at pH 7.5 and 25°C.

#### Radiochemistry.

##### Production of the radioactive precursor [<sup>13</sup>N]NO<sub>2</sub><sup>-</sup> by enzyme catalysis: general procedure.

Nitrogen-13 was produced in an IBA Cyclone 18/9 cyclotron via the <sup>16</sup>O(p,α)<sup>13</sup>N nuclear reaction. The target system consisted of an aluminum insert (2 mL) covered with havar foil (thickness 25 µm, Ø 29 mm) and with an aluminum vacuum foil (thickness 25 µm, Ø 23 mm). The target (containing 1.75 mL of ultrapure water, Type I water, ISO 3696) was irradiated with 18MeV protons. The beam current was

maintained at 20  $\mu\text{A}$  (pressure in the range 5–10 bar into the target during bombardment) to reach the desired integrated currents (0.1–0.5  $\mu\text{Ah}$ ). The resulting solution was transferred to a 10 mL vial and the activity was measured in a dose calibrator (Capintec CRC®-25 PET, New Jersey, USA). The final activities (corrected to the end of irradiation) were in the range 333–1110 MBq (9–30 mCi).

Enzymatic reduction of  $[^{13}\text{N}]\text{NO}_3^-$  to  $[^{13}\text{N}]\text{NO}_2^-$  was carried out with 6.72 mU of immobilized eNR packed into a plastic column. This insoluble preparation was incubated with 90  $\mu\text{L}$  of cyclotron produced  $^{13}\text{N}$  solution (which contained  $[^{13}\text{N}]\text{NO}_3^-$ ) in the presence of 10  $\mu\text{L}$  of 2.1 mM NADPH (0.21 mM final concentration) in 500 mM sodium phosphate buffer (final concentration = 50 mM; pH=7.5) under mild conditions (25°C and pH=7.5) for 4 min. Relative amounts of  $[^{13}\text{N}]\text{NH}_4^+$ ,  $[^{13}\text{N}]\text{NO}_2^-$  and  $[^{13}\text{N}]\text{NO}_3^-$  were measured by radio-HPLC. An Agilent 1200 series HPLC equipped with a quaternary pump, a multiple wavelength detector and a radiometric detector (Gabi, Raytest) was used. An HP Asahipak ODP-50 (5  $\mu\text{m}$ , 125x4 mm, Teknokroma, Spain) was used as stationary phase, and a solution containing additive for ionic chromatography (15 mL) in a mixture water/acetonitrile (86/14, V = 1L) basified to pH = 8.6 with 1M sodium hydroxide solution was used as the mobile phase at a flow rate of 1 mL/min. Simultaneous UV ( $\lambda = 254 \text{ nm}$ ) and isotopic detection were used.

### Two-step chemo-enzymatic synthesis of *S*- $[^{13}\text{N}]\text{nitrosogluthathione}$ ( $[^{13}\text{N}]\text{GSNO}$ ).

The preparation of  $[^{13}\text{N}]\text{GSNO}$  followed the synthetic protocol previously reported<sup>13</sup>, but the  $[^{13}\text{N}]\text{NO}_2^-$  used as labelling agent was enzymatically synthesized. A radioactive solution (300  $\mu\text{L}$ ) containing cyclotron produced  $[^{13}\text{N}]\text{NO}_3^-$  was incubated in a packed column equilibrated with 1 mM NADPH loaded with 175  $\mu\text{g}$  eNR per g of carrier (22mU of immobilized eNR determined as previously described) for 4 min; the resulting supernatant containing  $[^{13}\text{N}]\text{NO}_2^-$  was diluted with 1 mL of 10 mM sodium phosphate buffer (pH=7.5) and then flushed through an anion exchange cartridge (Sep-Pak® Accell Plus QMA, Waters) to selectively retain  $[^{13}\text{N}]\text{NO}_2^-$ . The column was further washed with distilled water (2 mL) and the QMA cartridge was dried with nitrogen gas for 15s. An acidic solution of the precursor glutathione (0.5 mL; 1 mM) was loaded into the cartridge and the nitrosation reaction was allowed to occur; the reaction mixture was finally eluted directly into a collection vial. The identification of  $[^{13}\text{N}]\text{GSNO}$  was performed by co-elution with reference standard using the same HPLC system described above; in this case, A Mediterranean SeaRP-18 column (5 $\mu\text{m}$ , 150 x 4.6mm, Teknokroma, Spain) was used as stationary phase and aqueous TFA solution/acetonitrile (95:5) was used as the mobile phase at a flow rate of 1 mL/min. Simultaneous UV ( $\lambda = 220 \text{ nm}$ ) and isotopic detection were used.

## Conclusions

Biochemical reactions have been exploited in many different synthetic reactions by chemists; however radiochemists have not paid enough attention to biocatalysis, and there are only a handful of examples where enzymes have been utilized in radiosynthetic schemes. Such under-exploitation is even more dramatic in the case of immobilized enzymes, despite the recent advances in heterogeneous biocatalysis.

Immobilized enzymes are exquisitely selective, highly active and stable, and simplify the process work-up, potentially yielding pure radiotracers that can be directly used for biomedical purposes. Hence, they can be anticipated as ideal tools for the preparation of radiotracers labelled with short-lived radionuclides. In this work we have applied for first time one eukaryotic nitrate reductase immobilized on a solid carrier to a radiochemical process. This immobilized enzyme has been able to selectively reduce  $[^{13}\text{N}]\text{NO}_3^-$  to  $[^{13}\text{N}]\text{NO}_2^-$  aided by NADPH as redox cofactor. We have demonstrated that by controlling the immobilization chemistry and physico-chemical properties of the carrier, optimal heterogeneous biocatalysts with high potential in synthetic chemistry can be achieved. Noteworthy, this work is one of the few examples where an immobilized enzyme has been applied for a radiochemical process and the first report so far of a two-step chemo-enzymatic route to synthesize a model radiotracers starting from a precursor ( $[^{13}\text{N}]\text{NO}_3^-$ ) directly produced in the cyclotron.

We have faced the challenge to immobilize an enzyme whose catalytic mechanism depends on several cofactors and conformational changes recovering enough activity and increasing its stability to catalyze several reaction cycles. The success of this work will so far open the doors to new application of enzymes in radiochemistry and will potentiate the use of other chemo-enzymatic designs for

the synthesis of novel radiotracers, even using short-lived isotopes. Successful enzyme immobilization will contribute to develop in flow radiochemical processes as well as to integrate radiochemical synthesis on-chip<sup>31-34</sup>.

## Acknowledgements

All the work has been supported by the RADIOMI project (EU FP7-PEOPLE-2012-ITN-RADIOMI). We would like to thank IKERBASQUE foundation for funding Dr. F. López-Gallego. We also acknowledge the support of COST Action CM1303 Systems Biocatalysis

## Notes and references

<sup>a</sup> Radiochemistry and Nuclear Imaging. CIC biomaGUNE, Paseo Miramon 182, 20009, San Sebastian (Spain)

<sup>b</sup> Radiochemistry Platform, Molecular Imaging Unit. CIC biomaGUNE, Paseo Miramon 182, 20009, San Sebastian (Spain)

<sup>c</sup> Biofunctional nanomaterials unit. CIC biomaGUNE, Paseo Miramon 182, 20009, San Sebastian (Spain)

<sup>d</sup> IKERBASQUE, Basque Foundation for Science, Bilbao (Spain)

Electronic Supplementary Information (ESI) available: [Thermal stability supporting data, fluorescence studies, scheme of chemo-enzymatic route to synthesize [<sup>13</sup>N]GSNO and SDS-PAGE of both soluble and immobilized ]. See DOI: 10.1039/b000000x/

1. K. Chen and X. Chen, *Semin. Oncol.*, 2011, **38**, 70.
2. J. S. Fowler and A. P. Wolf, *Acc. Chem. Res.*, 1997, **30**, 181.
3. C. Garcia-Galan, Á. Berenguer-Murcia, R. Fernandez-Lafuente and R. C. Rodrigues, *Adv. Synth. Catal.*, 2011, **353**, 2885.
4. G. Slegers, R. H. Lambrecht, T. Vandewalle, L. Meulewaeter and C. Vandecasteele, *J. Nucl. Med.*, 1984, **25**, 338.
5. M. Sasaki, M. Ikemoto, M. Mutoh, T. Haradahira, A. Tanaka, Y. Watanabe and K. Suzuki, *Appl. Radiat. Isot.*, 2000, **52**, 199.
6. M. E. Sergeev, F. Morgia, M. R. Javed, M. Doi and P. Y. Keng, *J. Mol. Catal. B: Enzym.*, 2013, **92**, 51.
7. M. E. Sergeev, F. Morgia, M. R. Javed, M. Doi and P. Y. Keng, *J. Mol. Catal. B: Enzym.*, 2013, **97**, 74.
8. V. Gómez-Vallejo, V. Gaja, K. B. Gona and J. Llop, *J. Labelled Compd. Radiopharmaceut.*, 2014, **57**, 244.
9. M. B. Cohen, L. Spolter, C. C. Chang, N. S. MacDonald, J. Takahashi and D. D. Bobinet, *J. Nucl. Med.*, 1974, **15**, 1192.
10. A. S. Gelbard, R. S. Benua, R. E. Reiman, J. M. McDonald, J. J. Vomero and J. S. Laughlin, *J. Nucl. Med.*, 1980, **21**, 988.
11. A. J. Cooper and A. S. Gelbard, *Anal. Biochem.*, 1981, **111**, 42.
12. J. Llop, V. Gómez-Vallejo, M. Bosque, G. Quincoces and I. Peñuelas, *Appl. Radiat. Isot.*, 2009, **67**, 95.
13. V. Gómez-Vallejo, K. Kato, I. Oliden, J. Calvo, Z. Baz, J. I. Borrell and J. Llop, *Tetrahedron Lett.*, 2010, **51**, 2990.
14. V. Gómez-Vallejo, K. Kato, M. Hanyu, K. Minegishi, J. I. Borrell and J. Llop, *Bioorg. Med. Chem. Lett.*, 2009, **19**, 1913.
15. V. Gaja, V. Gomez-Vallejo, M. Puigivila, C. Perez-Campana, A. Martin, A. Garcia-Osta, T. Calvo-Fernandez, M. Cuadrado-Tejedor, R. Franco and J. Llop, *Mol. Imaging Biol.*, 2014, **16**, 538.
16. V. Gomez-Vallejo, J. I. Borrell and J. Llop, *Eur. J. Med. Chem.*, 2010, **45**, 5318.
17. S. M. Joshi, V. Gomez-Vallejo and J. Llop, Pamplona, Spain, 2014.
18. K. Fischer, G. G. Barbier, H.-J. Hecht, R. R. Mendel, W. H. Campbell and G. Schwarz, *The Plant Cell*, 2005, **17**, 1167.
19. R. B. Mellor, J. Ronnenberg, W. H. Campbell and S. Diekmann, *Nature*, 1992, **355**, 717.
20. C. Mateo, O. Abian, R. Fernandez-Lafuente and J. M. Guisan, *Biotechnol. Bioeng.*, 2000, **68**, 98.
21. F. C. Wedler and F. M. Hoffmann, *Biochemistry*, 1974, **13**, 3207.
22. F. Facchiano, R. Ragone, M. Porcelli, G. Cacciapuoti and G. Colonna, *Eur. J. Biochem.*, 1992, **204**, 473.
23. J. Rocha-Martin, D. Vega, J. Bolivar, C. Godoy, A. Hidalgo, J. Berenguer, J. Guisan and F. Lopez-Gallego, *BMC Biotechnol.*, 2011, **11**, 101.
24. V. Sachdeva and V. Hooda, *Talanta*, 2014, **124**, 52.
25. B. C. Pessela, R. Munilla, L. Betancor, M. Fuentes, A. V. Carrascosa, A. Vian, R. Fernandez-Lafuente and J. M. Guisan, *J. Chromatogr. A*, 2004, **1034**, 155.
26. R. Fernandez-Lafuente, C. M. Rosell, V. Rodriguez, C. Santana, G. Soler, A. Bastida and J. M. Guisan, *Enzyme Microb. Technol.*, 1993, **15**, 546.
27. M. Fuentes, B. C. C. Pessela, J. V. Maquiese, C. Ortiz, R. L. Segura, J. M. Palomo, O. Abian, R. Torres, C. Mateo, R. Fernández-Lafuente and J. M. Guisán, *Biotechnol. Prog.*, 2004, **20**, 1134.
28. K. Arnold, L. Bordoli, J. Kopp and T. Schwede, *Bioinformatics*, 2006, **22**, 195.
29. I. Walsh, G. Minervini, A. Corazza, G. Esposito, S. C. E. Tosatto and F. Fogolari, *Bioinformatics*, 2012, **28**, 2189.
30. M. M. Bradford, *Anal. Biochem.*, 1976, **72**, 248.
31. C. Rensch, S. Lindner, R. Salvamoser, S. Leidner, C. Bold, V. Samper, D. Taylor, M. Baller, S. Riese, P. Bartenstein, C. Wangler and B. Wangler, *Lab on a Chip*, 2014, **14**, 2556.

32. H. Zhang, M. V. Cantorias, N. Pillarsetty, E. M. Burnazi, S. Cai and J. S. Lewis, *Nucl. Med. Biol.*, 2012, **39**, 1182.
33. S. Lu, J.-H. Chun and V. W. Pike, *J. Labelled Comp. Radiopharm.*, 2010, **53**, 234.
34. P. Y. Keng, S. Chen, H. Ding, S. Sadeghi, G. J. Shah, A. Dooraghi, M. E. Phelps, N. Satyamurthy, A. F. Chatziioannou, C.-J. C. Kim and R. M. van Dam, *Proc. Natl. Acad. Sci. U. S. A.*, 2012, **109**, 690.